Astronomy & Astrophysics manuscript no. output
January 20, 2026

Optimizing the global detection of solar-like oscillations

Tuning the frequency range for asteroseismic detection predictions and searches

Mikkel N. Lund[1,⋆] and William J. Chaplin[2,⋆⋆]

[1] Stellar Astrophysics Centre, Department of Physics and Astronomy, Aarhus University, Ny Munkegade 120, DK-8000 Aarhus C, Denmark

[2] School of Physics and Astronomy, University of Birmingham, Birmingham, B15 2TT, United Kingdom

Received XX, YY

ABSTRACT

Context. A well-established methodology exists for predicting the detectability of solar-like oscillations, which has seen extensive application supporting target selection strategies for space-based photometric missions. The method assesses the probability of making an asteroseismic detection based on the expected global signal-to-noise ratio (SNR) of the observed signal due to the oscillations against the broadband background due to shot noise and granulation. Known stellar parameters are used to compute the expected oscillation and granulation signal, while instrumental specifications and the apparent brightness of the target are used to compute the expected shot noise.

Aims. Here, we aim to explore whether there is an optimal choice for the range in frequency, W, over which the global SNR is determined. The observed power in the solar-like oscillations is assumed to follow a Gaussian-like envelope of full-width at half maximum $\Gamma_{\rm env}$, centred on the frequency of maximum oscillation power. It has been common practice to set $W \simeq 2\Gamma_{\rm env}$ when making detection predictions.

Methods. We make numerical predictions of the global SNR and resulting detection probabilities for a range of underlying stellar and observational parameters, adopting different choices for the width using $W = \alpha\Gamma_{\rm env}$, where α is a multiplicative coefficient that controls the width. We also explore the impact of this choice on detection yields across an ensemble of targets, using a sample of bright solar-like oscillators observed by TESS as a representative example.

Results. We find that the commonly adopted value of $\alpha \simeq 2$ is a sub-optimal choice, and that adopting a range with $\alpha \simeq 1.2$ maximises the probability of detection. There can also be a substantial impact on the predicted detection yield across a sample of stars.

Conclusions. In summary, we recommend the adoption of a range $W \simeq 1.2\Gamma_{\rm env}$, not only in computations of the detection probabilities but also in actual searches for oscillations in real data based on testing the significance of excess mode power, since its adoption will also optimise the probability of making robust detections.

Key words. Asteroseismology – Stars: oscillations (including pulsations) – Stars: late-type – Methods: statistical

1. Introduction

Solar-like oscillations have now been detected in hundreds of cool main-sequence and subgiant stars, and in thousands of red giants (e.g., see Chaplin & Miglio 2013; García & Ballot 2019). Because the oscillation parameters follow scaling relations that depend on fundamental stellar properties to very good approximation (e.g., see Basu & Chaplin 2017), it is possible to make straightforward predictions of the detectability of the oscillations if the noise budget of the observations is known; and to use these known characteristics to tune codes that seek to detect signatures of oscillations in the data. The ability to make such predictions is central to target selection strategies, in particular those for space-based photometric missions. It can inform decisions on the selection of observing fields, specific targets, and observing durations, etc., in order to fulfil mission-specific requirements on detection yields that support specific science goals.

In this paper, we present an optimisation of the detection prediction methodology of Chaplin et al. (2011). This approach was developed to inform asteroseismic target selection strategies for the NASA *Kepler* mission, and has since been used for the K2 (Chaplin et al. 2015; Lund et al. 2016, 2024), TESS (Campante et al. 2016; Schofield et al. 2019; Hey et al. 2024) and CHEOPS (Moya et al. 2018) missions, and more recently in preparations for the upcoming ESA PLATO mission (Goupil et al. 2024). The optimisation is of the choice of frequency range over which to calculate the global signal-to-noise ratio (SNR) of the oscillations in the frequency power spectrum of the data. This optimal choice of range is then also relevant to the actual searches for oscillations in real data, since its adoption optimises the probability of making robust detections.

The layout of the rest of the paper is as follows. In Sect. 2, we recap the key elements of the methodology. Sect. 3 contains the main results of the paper. Sect. 3.1 presents formulae to describe the integrated oscillations power and global SNR over different ranges in frequency. We then use these formulae in Sect. 3.2 to show that the commonly adopted choice of frequency range is

⋆ mikkelnl@phys.au.dk
⋆⋆ w.j.chaplin@bham.ac.uk

sub-optimal, and provide updated guidance on the best range to adopt in detection predictions and in actual searches for the oscillations. We finish in Sect. 4 with our main conclusions.

2. The detection recipe

We begin by summarising the key elements of the Chaplin et al. (2011) approach. First, we follow the well-established convention of assuming that when smoothed in frequency, the observed power in the solar-like oscillations follows a Gaussian-like envelope centred on the frequency of maximum oscillation power, $\nu_{\rm max}$. We may then write the power spectral density $P(\nu)$ of the envelope as:

$$P(\nu) = H_{\rm env} \exp\left[-4\ln 2\left(\frac{\nu-\nu_{\rm max}}{\Gamma_{\rm env}}\right)^2\right], \quad (1)$$

where $H_{\rm env}$ and $\Gamma_{\rm env}$ are, respectively, the height and full width at half maximum (FWHM) of the envelope. The total area under the envelope corresponds to the total detected mean-square power in the oscillations, and is given by:

$$P_{\rm tot} = \left(\frac{\pi}{4\ln 2}\right)^{1/2} H_{\rm env}\Gamma_{\rm env}. \quad (2)$$

Predictions of $P_{\rm tot}$ may be made for a given stellar target using well-established scaling relations for the oscillation parameters (e.g., see Basu & Chaplin 2017 for further details).

The Chaplin et al. (2011) detection methodology then uses the global SNR in the oscillations, as defined by:

$$\mathrm{SNR}_{\rm tot} = \frac{P_{\rm tot}}{B_{\rm tot}}, \quad (3)$$

where $B_{\rm tot}$ is the total background power across the frequency range occupied by the modes. In what follows, we denote this range as W.

The background has contributions from shot and other instrumental noise, as well as stellar granulation. We assume that the underlying limit spectra arising from these noise sources—that is, the spectra that would be given by an infinite number of realisations of the data—are either constant or vary slowly across the frequency range of interest. We then specify an average background power spectral density $\bar{b}$, from which it follows that:

$$B_{\rm tot} = \bar{b}W. \quad (4)$$

Estimates of the noise will depend on the apparent brightness of the target, and the instrumental response and sensitivity; while the granulation contribution may be computed using scaling relations that depend on fundamental stellar properties (e.g., Kallinger et al. 2014).

When the time-domain observations span a duration T, the number of independent frequency bins N that span the range W will be

$$N = WT. \quad (5)$$

The power spectral density within any independent bin will follow χ^2 2 d.o.f. statistics about the underlying limit spectrum (Appourchaux 2014). The global SNR, which is computed over N bins, then follows χ^2 $2N$ d.o.f. statistics. With predicted estimates of the underlying $P_{\rm tot}$ and total noise $B_{\rm tot}$ in hand for a particular target, we may then calculate the probability $p_{\rm final}$ that the observed SNR would exceed some false-alarm threshold $p_{\rm false}$, consistent with the statistics defined above (Appourchaux 2004).

It has been common practice to set $W \simeq 2\Gamma_{\rm env}$, so that the full range encompases most (strictly just over 95 %) of the total oscillation power $P_{\rm tot}$. We now go on to show that this is a sub-optimal choice.

3. Optimisation of the full range W

3.1. Generalised formulae for different ranges W

To test how the global SNR and detection probability $p_{\rm final}$ depend on the choice of range W, we begin by presenting formulae that capture differing fractions of the full Gaussian envelope. We define a coefficient α that controls the range according to:

$$W = \alpha\Gamma_{\rm env}. \quad (6)$$

Previous practice has therefore been consistent with setting $\alpha \simeq 2$.

The integrated area of the Gaussian envelope contained within a symmetric frequency range W about $\nu_{\rm max}$ is

$$P_{\rm tot}(W) = \int_{\nu_{\rm max}-W/2}^{\nu_{\rm max}+W/2} P(\nu)\,{\rm d}\nu. \quad (7)$$

Evaluating the integral gives

$$P_{\rm tot}(W) = P_{\rm tot}\,\mathrm{erf}\left(\frac{W\sqrt{2\ln 2}}{\Gamma_{\rm env}}\right), \quad (8)$$

where $P_{\rm tot}$ is the full Gaussian area given by Eq. 2. We may rewrite the error function (erf) in the above in terms of α alone (cf. Eq. 6), and changing the independent variable specifying the dependence of the integral on the selected range from W to α, we have:

$$P_{\rm tot}(\alpha) = P_{\rm tot}\,\mathrm{erf}\left(\alpha\sqrt{\ln 2}\right). \quad (9)$$

The global SNR is:

$$\mathrm{SNR}_{\rm tot}(\alpha) = \frac{P_{\rm tot}(\alpha)}{B_{\rm tot}(\alpha)}, \quad (10)$$

which we may write explicitly as:

$$\mathrm{SNR}_{\rm tot}(\alpha) = \frac{P_{\rm tot}}{\alpha\Gamma_{\rm env}\bar{b}(\alpha)}\,\mathrm{erf}\left(\alpha\sqrt{\ln 2}\right). \quad (11)$$

To help understand the results that follow, it is also instructive to express the formulae in terms of an average power spectral density $\bar{P}(\alpha)$ across the range defined by α, that is,

$$\bar{P}(\alpha) = P_{\rm tot}(\alpha)/W \equiv \left(\frac{P_{\rm tot}}{\alpha\Gamma_{\rm env}}\right)\mathrm{erf}\left(\alpha\sqrt{\ln 2}\right). \quad (12)$$

The global SNR may then be written in the form:

$$\mathrm{SNR}_{\rm tot}(\alpha) = \frac{\bar{P}(\alpha)}{\bar{b}(\alpha)}, \quad (13)$$

from which it is clear that it scales directly with the average power spectral density.

It is obvious that by increasing α, and hence W, the average power spectral density $\bar{P}(\alpha)$ and the global SNR will decrease. However, this must be tensioned against the commensurate increase in N, and hence the number of degrees of freedom governing the statistics of the global SNR. At fixed SNR, the larger N, the higher will be the detection probability $p_{\rm final}$. In short, the SNR required for a detection will be reduced. The combination of these opposing effects suggests that there will be an optimal choice for α that provides the best compromise.

3.2. The optimal frequency range

The left-hand panel of Fig. 1 shows how the global SNR varies with α for different assumed values of $\mathrm{SNR}_{\mathrm{tot}}(2) \in [0.02, 0.10]$ (see plot annotation), with the vertical dotted line marking the standard value of $\alpha = 2$. The plotted lines show the expected trend: $\mathrm{SNR}_{\mathrm{tot}}(\alpha)$ decreases with increasing α. The right-hand panel plots the corresponding detection probabilities, p_{final}, assuming a false-alarm threshold of $p_{\mathrm{false}} = 0.01$. We used $\nu_{\mathrm{max}} = 2000\,\mu$Hz and calculated the envelope FWHM using the well-established relation $\Gamma_{\mathrm{env}} = 0.66\nu_{\mathrm{max}}^{0.88}$ (Mosser et al. 2012). We also assumed observations of duration $T = 1$ month, from which we calculated N for each value of α using Eqs. 5 and 6.

The right-hand panel reveals a maximum in the curves at a value of $\alpha \simeq 1.2$, marked with the dashed line. The standard value of $\alpha = 2$ is seen to be sub-optimal. Other choices of ν_{max} and T give essentially the same results, with some very small scatter in the optimal value for α. The largest gain appears to come at intermediate detection probabilities.

This behaviour is illustrated in Fig. 2, which shows how the change $\Delta p_{\mathrm{final}}$ between $\alpha = 1.2$ and 2.0 varies with ν_{max}, p_{final} (left-hand column) and $\mathrm{SNR}_{\mathrm{tot}}(2)$ (right-hand column). The top row shows results for $T = 1$ month, and the bottom row for $T = 6$ months. The right-hand panel reveals a well-constrained optimal region in ν_{max}-SNR space. To the right of this region, the detection probability is already high, meaning little if any gain is to be had through changing α. Note that the upper right-hand half of the plot will in practice not contain real stars, because the maximum mode amplitudes and hence P_{tot} decrease strongly with increasing ν_{max}. To the left of the optimal region, the SNR is so low that there is a negligible impact on the probability from changing α. The optimal region moves to higher SNR at lower ν_{max} because $N \propto \Gamma_{\mathrm{env}} \propto \nu_{\mathrm{max}}^{0.88}$ drops, meaning a higher SNR is required to give similar gains in probability. It is also shifted to higher SNR at lower T, for the same reason. We note that increasing the false-alarm probability p_{false} has the effect of moving the ridge in $\Delta p_{\mathrm{final}}$ from Fig. 2 to lower $\mathrm{SNR}_{\mathrm{tot}}(2)$ values, and vice versa for a decreased p_{false}.

Figure 3 shows results of detectability predictions for a sample of bright stars observed by TESS (Ricker et al. 2015). Specifically, we adopted the $V \leq 6$ stars from the TESS Luminaries Sample (Lund et al. 2025), including also the sample of bright evolved stars (their Fig. 1). Detectability predictions were made using the `ATL3` tool of Hey et al. (2024)[1]—which implements the Chaplin et al. (2011) methodology—assuming a single sector of TESS observations ($T \simeq 1$ month), 120-sec cadence data, a false-alarm probability of 5%, and using input values of T_{eff}, $\log g$, and R from Gaia DR3's `gspphot` (Gaia Collaboration et al. 2023). Figure 3 shows the same structure as in the above calculations and plots, as well as the expected *absence* of stars in the upper right-hand half of the ν_{max}-SNR plot.

For this specific sample, the predicted yield for $p_{\mathrm{final}} \geq 0.90$ increased by ~12% when changing from $\alpha = 2$ to 1.2, and by ~5% for $p_{\mathrm{final}} \geq 0.99$. This illustrates the benefits that accrue when considering the returns from a target ensemble. The improvement in the predicted yield will naturally depend heavily on the sample—if, for example, a significantly longer observing duration is considered, many stars in a bright sample like the TESS one considered here would move to higher values of $\mathrm{SNR}_{\mathrm{tot}}(2)$ (to the right in Fig. 2), and the relative improvement in p_{final} from changing α would decrease. Similarly, for a sample of dimmer stars, many would have very low $\mathrm{SNR}_{\mathrm{tot}}(2)$ values and a longer observing duration T would be needed to see a significant relative change in p_{final} from changing α.

[1] Updated with a TESS-specific bolometric correction for mode amplitudes (Lund 2019).

4. Conclusion

We have presented a straightforward optimisation to the asteroseismic detection prediction recipe of Chaplin et al. (2011), tuning the frequency range used for assessing the significance of excess power from solar-like oscillations. Instead of the range normally adopted—corresponding to twice the FWHM of the oscillation envelope (i.e., $2\Gamma_{\mathrm{env}}$), we find that adopting a range of $1.2\Gamma_{\mathrm{env}}$ maximises the probability of detection.

Depending on the sample considered, this optimisation can have a substantial effect on the predicted detection yield. We therefore recommend the modification be implemented in target selection and detection prediction efforts for future missions suitable for asteroseismology, including the ESA PLATO Mission (Goupil et al. 2024) and the NASA Roman Space Telescope (Weiss et al. 2025). Furthermore, it is important to add that using our recommended range will also be beneficial for codes that actually analyse the data to detect solar-like oscillations, based on testing the significance of excess mode power (e.g., Appourchaux 2004; Lund et al. 2012; Bell et al. 2019; Viani et al. 2019; Nielsen et al. 2022), since its adoption will also optimise the probability of making robust detections.

Acknowledgements. MNL acknowledges support from the ESA PRODEX programme (PEA 4000142995). WJC acknowledges the support of the UK Space Agency. This research has made use of NASA's Astrophysics Data System Bibliographic Services.

References

Appourchaux, T. 2004, A&A, 428, 1039
Appourchaux, T. 2014, in Asteroseismology, ed. P. L. Pallé & C. Esteban, 123
Basu, S. & Chaplin, W. J. 2017, Asteroseismic Data Analysis: Foundations and Techniques
Bell, K. J., Hekker, S., & Kuszlewicz, J. S. 2019, MNRAS, 482, 616
Campante, T. L., Schofield, M., Kuszlewicz, J. S., et al. 2016, ApJ, 830, 138
Chaplin, W. J., Kjeldsen, H., Bedding, T. R., et al. 2011, ApJ, 732, 54
Chaplin, W. J., Lund, M. N., Handberg, R., et al. 2015, PASP, 127, 1038
Chaplin, W. J. & Miglio, A. 2013, ARA&A, 51, 353
Gaia Collaboration, Vallenari, A., Brown, A. G. A., et al. 2023, A&A, 674, A1
García, R. A. & Ballot, J. 2019, Living Reviews in Solar Physics, 16, 4
Goupil, M. J., Catala, C., Samadi, R., et al. 2024, A&A, 683, A78
Hey, D., Huber, D., Ong, J., Stello, D., & Foreman-Mackey, D. 2024, arXiv e-prints, arXiv:2403.02489
Kallinger, T., De Ridder, J., Hekker, S., et al. 2014, A&A, 570, A41
Lund, M. N. 2019, MNRAS, 489, 1072
Lund, M. N., Basu, S., Bieryla, A., et al. 2024, A&A, 688, A13
Lund, M. N., Chaplin, W. J., Casagrande, L., et al. 2016, PASP, 128, 124204
Lund, M. N., Chaplin, W. J., & Kjeldsen, H. 2012, MNRAS, 427, 1784
Lund, M. N., Chontos, A., Grundahl, F., et al. 2025, A&A, 701, A285
Mosser, B., Elsworth, Y., Hekker, S., et al. 2012, A&A, 537, A30
Moya, A., Barceló Forteza, S., Bonfanti, A., et al. 2018, A&A, 620, A203
Nielsen, M. B., Hatt, E., Chaplin, W. J., Ball, W. H., & Davies, G. R. 2022, A&A, 663, A51
Ricker, G. R., Winn, J. N., Vanderspek, R., et al. 2015, Journal of Astronomical Telescopes, Instruments, and Systems, 1, 014003
Schofield, M., Chaplin, W. J., Huber, D., et al. 2019, ApJS, 241, 12
Viani, L. S., Basu, S., Corsaro, E., Ball, W. H., & Chaplin, W. J. 2019, ApJ, 879, 33
Weiss, T. J., Downing, N. J., Pinsonneault, M. H., et al. 2025, ApJ, 987, 181

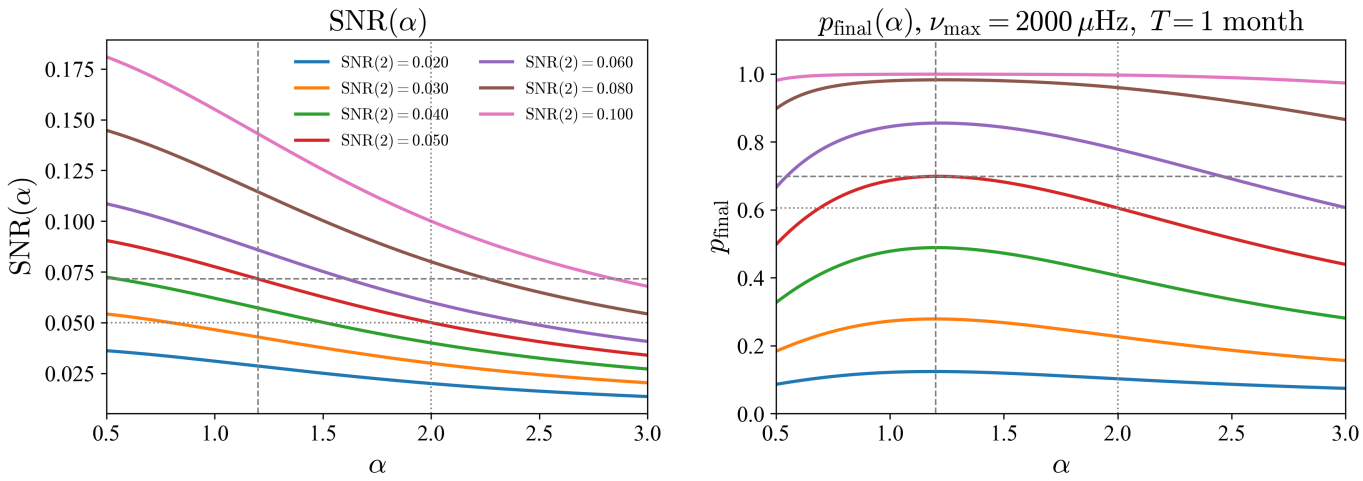

Fig. 1: Left: Variation of SNR values with α, for different assumed values of $\mathrm{SNR}_{\mathrm{tot}}(2) \in [0.02, 0.10]$ (see plot annotation), with the vertical dotted line marking the standard value of $\alpha = 2$ and the vertical dashed line marking the optimal value of $\alpha \simeq 1.2$. Horizontal dotted/dashed lines mark the corresponding intersection with the red curve, having $\mathrm{SNR}_{\mathrm{tot}}(2) = 0.050$. Right: the corresponding detection probabilities, p_{final}, for $\nu_{\mathrm{max}} = 2000\,\mu$Hz and $T = 1$ month.

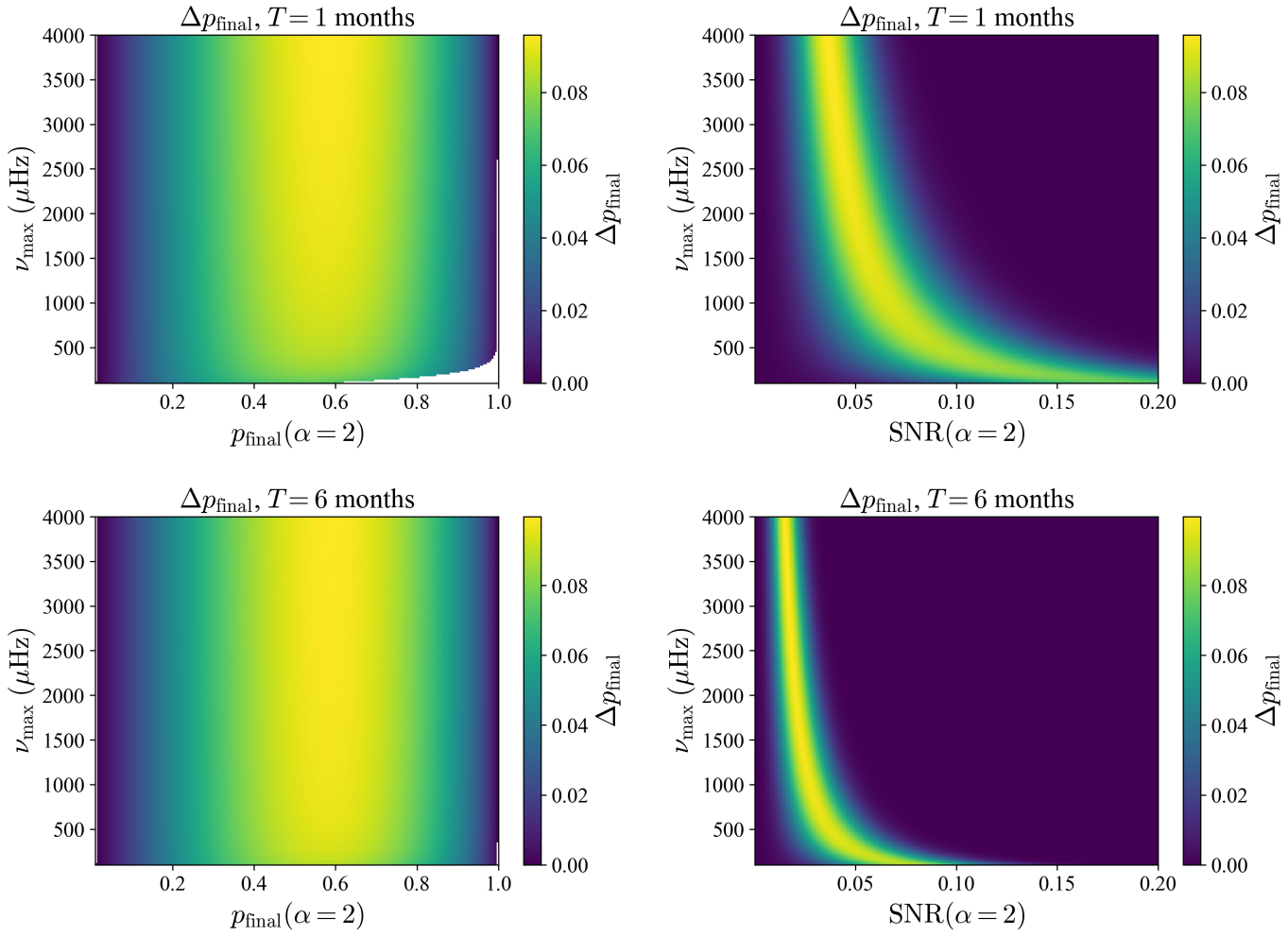

Fig. 2: Results on how the change $\Delta p_{\mathrm{final}}$ between $\alpha = 1.2$ and 2.0 varies with ν_{max}, p_{final} (left-hand column) and $\mathrm{SNR}_{\mathrm{tot}}(2)$ (right-hand column). The top row shows results for $T = 1$ month, and the bottom row for $T = 6$ months.

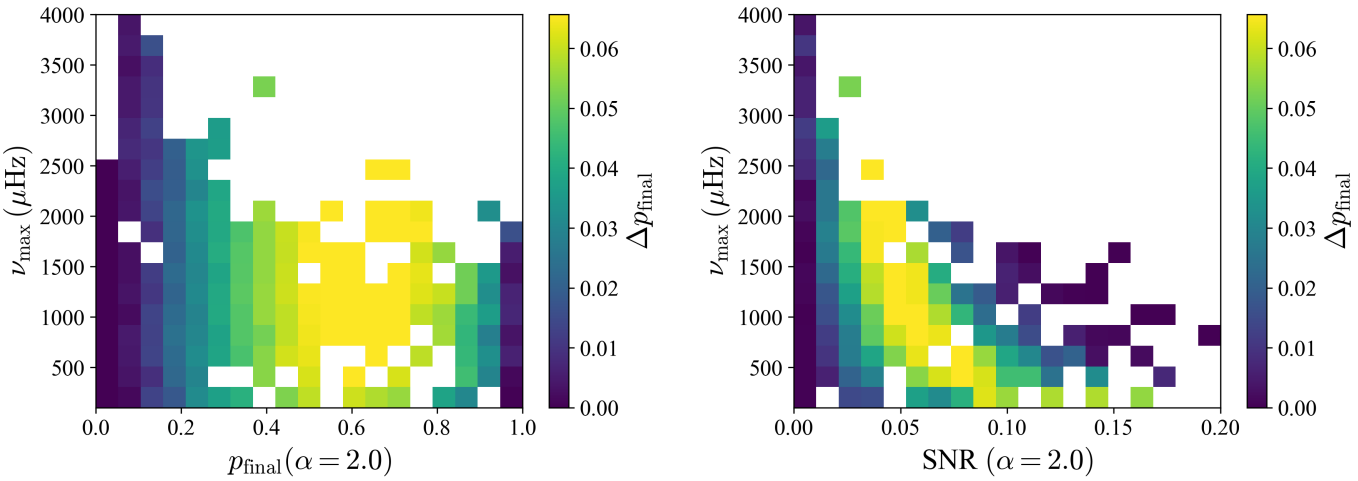

Fig. 3: Results for predictions using the bright TESS stars from the TESS Luminaries Sample (Lund et al. 2025), assuming a single sector of TESS observations ($T \simeq 1$ month), 120-sec cadence data, a false-alarm probability of 5%, and using input values of $T_{\rm eff}$, $\log g$, and R from Gaia's DR3 `gspphot`.